LANGMUIR

pubs.acs.org/Langmuir Article

Effects of Water Content on the Transport and Thermodynamic Properties of Phosphonium Ionic Liquids

Igor Stanković,* Miljan Dašić, Mateja Jovanović, and Ashlie Martini

Cite This: *Langmuir* 2024, 40, 9049−9058 Read Online

ACCESS | Metrics & More | Article Recommendations

ABSTRACT: We present a numerical investigation of the influence of water content on the dynamic properties of a family of phosphonium-based room-temperature ionic liquids. The study presents a compelling correlation between structural changes in water−ionic liquid solutions and thermodynamic and transport properties across diverse systems. The results for phosphonium ionic liquids are compared with 1-butyl-3-methylimidazolium hexaphosphate ([bmim]PF_6) as a reference. Through this approach, phosphonium cation structure-related characteristics can be identified and placed within the broader context of ionic liquids. These insights are underpinned by observed changes in interaction energy, boiling point, diffusion rate, and viscosity, highlighting the crucial role of water molecules in weakening the strength of interactions between ions within the ionic liquid. The investigation also explains temperature-dependent trends in phosphonium cations, showing that alkyl group length and molecular symmetry are important tuning parameters for the strength of Coulomb interactions. These results contribute to a refined understanding of phosphonium ionic liquid behavior in the presence of water, offering valuable insights for optimizing their use in diverse fields.

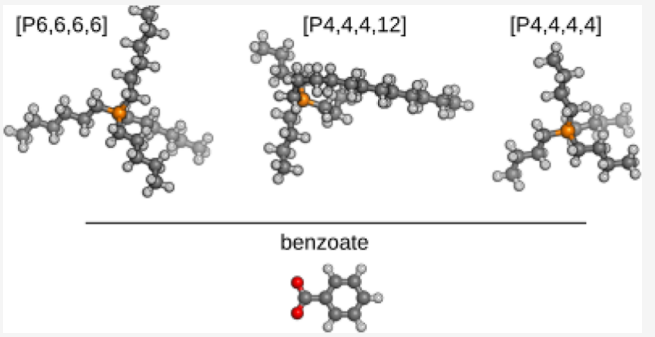

INTRODUCTION

Ionic liquids (ILs) include a class of salts characterized by their ability to remain in a liquid state at room temperature, with a melting point below room temperature (300 K). Through the high versatility of large asymmetric and irregularly shaped organic or inorganic cations and anions, ILs possess unique physicochemical properties that make them relevant for wide-ranging modern applications. These properties include negligible vapor pressure, exceptional thermal stability, high viscosity, significant ion conductivity, a wide electrochemical window, and adjustable polarity.[1,2] Such attributes have led to the exploration of ILs in a diverse range of fields, including lubrication.[3−5] Hence, it would be advantageous if we could deduce relations between the molecular structure, transport, and lubrication properties of ILs.

ILs utilized for lubrication purposes incorporate different types of anions, both organic and inorganic, as well as various cations. Among the commonly employed cations are those based on ammonium, phosphonium,[6] imidazolium,[1] or pyridinium.[7] Notably, recent studies have highlighted the potential of phosphonium ILs for lubrication due to several advantageous characteristics.[3,8−10] Phosphonium ILs have been found to exhibit reduced wear and friction compared to commonly used oils, and even ammonium and imidazolium ILs.[8,11,12] Phosphonium ILs have also been reported to possess excellent resistance to corrosion and tribo-corrosion.[13] Their low volatility[9] enables recycling and reusability without volume loss, highlighting phosphonium ILs as leading candidates for lubricant applications. The length of the alkyl chain in cations has been found to influence the viscosity, melting point, and pressure-viscosity coefficients of ILs.[3,10] The influence of cationic alkyl chain length on the tribological properties of ILs in lubrication has been investigated.[1,6,12,14−16] Interestingly, Minami[12] observed a decrease in the coefficient of friction (COF) from 0.25 to 0.15 with increasing alkyl chain length (nC = 2 to 12), while Dold et al.[1] observed an increase in COF from 0.025 to 0.1. Studies have also considered ILs with the same cations but different anions. ILs change wetting behavior depending on the anion size,[6,14−16] from the absence of wetting to partial or complete wetting.

Water is commonly employed during the synthesis of ILs, and many ILs have a strong affinity for water. Consequently, the residual water in ILs significantly influences various properties such as density, viscosity, polarity, conductivity,

Received: January 29, 2024
Revised: March 28, 2024
Accepted: April 1, 2024
Published: April 19, 2024

https://doi.org/10.1021/acs.langmuir.4c00372
Langmuir 2024, 40, 9049−9058

and solubility.[17,18] The solubility of ILs in water is particularly important for reducing emulsification in water-based lubricants. Both theoretical and experimental studies comparing different ILs based on the symmetric phosphonium [P4,4,4,4] cation revealed that solubility depends on the choice of anion.[19,20] Molecular dynamics (MD) simulations investigating the mixing behavior between phosphonium ILs with chloride and acetate anions and water showed that, while the anions were well solvated due to their small size, only the smallest cation [P2,2,2,2] was fully miscible with water, forming a homogeneous binary solution.[21] The analysis emphasized electrostatic nature of cation−anion and anion−water interactions, with van der Waals interactions playing a dominant role in cation−water interactions.[20]

Understanding the properties of water−ionic liquid systems is challenging due to different mechanisms and structural units that can contribute to the interaction, such as ion solvation, ion association, and numerous dynamic properties in the system. Molecular dynamics is a powerful technique to examine electrolyte properties because a direct correlation between the atomistic level information and macroscopic properties can be obtained.[6] Molecular dynamics simulations were carried out on four ILs based on the combinations of four different cations ([P6,6,6,6], [P4,4,4,12], [P4,4,4,4], and 1-butyl-3-methylimidazolium [bmim]) with two anions benzoate [benz] and hexafluorophosphate PF_6.[6,9,22] Both anions and [bmim] cations have similar molar masses. They are also roughly 50% lighter than the [P4,4,4,4] cation. Previous research has focused on the physical properties of imidazolium hydrophilic ionic liquid (IL) and water mixtures.[23−25] The cation side chain modification in imidazolium-based ILs was reported to significantly influence its aggregation in the presence of water.[26,27] Also, water-induced cluster formation could disrupt ion interactions[28] and, for mixtures with 70 mol % or more of water, the imidazolium-based IL systems behave as aqueous solutions.[28,29] Therefore, comparing anions and cations with systematically varied shapes and sizes is useful for studies aimed at understanding the effect of molecular shape and mobility on tribological and mixing properties of ILs in the presence of water.

Here, we present a comprehensive computational study of the influence of water concentration on the structure of IL as well as on the evolution of water−IL interactions. In particular, we perform molecular dynamics simulations for dilute water/IL systems for different anion types and phosphonium-based cations with a range of alkyl-chain lengths. The role of the symmetry and size of the phosphonium cation is examined. The results for three phosphonium-based ionic liquids are also compared with an imidazolium ionic liquid with a comparable molecular weight. The set of considered ionic liquid cation−anion pairs is depicted in Figure 1.

MATERIALS AND METHODS

Since the cation alkyl chain length affects the water affinity of ILs, the simulations include three different phosphonium cations, [P6,6,6,6], [P4,4,4,12], and [P4,4,4,4], in combination with benzoate [Benz] anion. The results for the phosphonium family are compared with the behavior of 1-butyl-3-methylimidazolium hexafluorophosphate ([bmim]PF_6) ionic liquid. Each simulation consisted of one ionic liquid homogeneously mixed with water. The initial configurations were obtained by random placement of ions $N_c = N_A = 80$ for [bmim]PF_6, 160 for [P6,6,6,6][benz] and [P4,4,4,12][benz], and 205 for [P4,4,4,4][benz] ILs into a cubic simulation box. The number of water molecules was adjusted accordingly to obtain the following

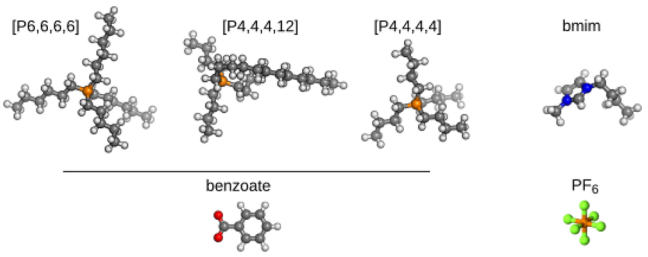

Figure 1. Snapshots of the molecular models of the three phosphonium ([P6,6,6,6], [P4,4,4,12], and [P4,4,4,4]) and 1-butyl-3-methylimidazolium [bmim] cations, as well as benzoate [benz] and PF_6 anions used in the simulations of ILs. Sphere colors correspond to atom type: white, H; gray, C; orange, P; red, O; green F; blue N. The images are generated with LigParGen.[30,31]

mass volume fractions: $N_{H_2O} = 2590$ corresponding to the concentration of $45\%_{w,IL}$, $N_{H_2O} = 1520$ $60\%_{w,IL}$, and $N_{H_2O} = 304$ for $87\%_{w,IL}$.

The interatomic interactions within ILs were characterized using the OPLS-AA force field derived from LigParGen.[30,31] The intramolecular forces inside the water were calculated with the SPC/*E* potential.[32,33] The interactions between ILs and water were calculated using the common Lorentz−Berthelot mixing rules.[34,35] In principle, the electronic polarizability of water and ionic liquid molecules should be considered to have an accurate depiction of their interactions and dynamics. However, previous simulations utilizing nonpolarizable water and IL models[6,36,37] have effectively captured crucial characteristics of the water−IL mixture, hence justifying the adequacy of the force fields adopted in this study. The value of the surface tension, as well as viscosity[38] and self-diffusion,[39] for the SPC/E models is found to be in reasonably good agreement with experiment.[32]

MD simulations were conducted using the open-source LAMMPS package[40] with a time step of 1 fs, and a typical length of simulation before property data were collected was 0.5 ns, which was sufficient for the energy to reach a steady state. To maintain the desired temperature, a Nosé−Hoover thermostat was utilized, while the velocity-Verlet algorithm was applied to solve the equations of motion.[41,42] The constant pressure (1 bar) simulations were performed with a barostat coupled to the overall box volume. The external pressure was specified as a scalar (isobaric ensemble). The damping parameters for the thermostat and barostat were 10 fs and 1 ps, respectively.

RESULTS

Impact of Water on the Ionic Liquid Structure. Figure 2 illustrates the time-averaged interaction energies (u) between water and ions in four different ILs after a steady state was reached. These energies represent the combined effects of Coulombic and van der Waals forces between water and the surrounding ions. The corresponding potential energy values were derived from MD simulations of the ILs, as explained in the Materials and Methods section. We compare simulation results in equilibrium for water/IL systems for a concentrated $99.5\%_w$ and diluted $60\%_{w,IL}$ with water. The differences between the interaction energies of anions and cations with water are also outlined in Figure 3. These results reveal that the interaction energies between water and anions are 2−4 times higher than those between water and cations. This finding is consistent with previous molecular dynamics observations for imidazolium ILs.[27]

In the case of phosphonium ILs, the strength of the water−cation interaction decreased with the molecular weight of the cation from 7 kcal/mol for [P4,4,4,4][benz] to 2.8 kcal/mol for [P6,6,6,6][benz], considering a highly concentrated $99.5\%_w$

https://doi.org/10.1021/acs.langmuir.4c00372
Langmuir 2024, 40, 9049−9058

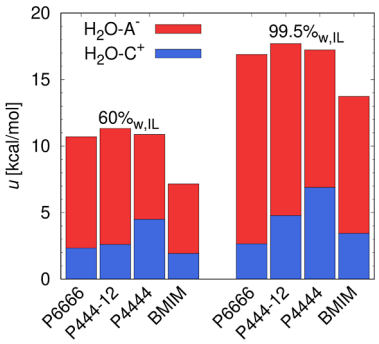

Figure 2. Interaction energies of water with cations, $u_{H_2O-C^+}$, and anions, $u_{H_2O-A^-}$, in four different simulated ILs. The results are shown for phosphonium benzoate [P6,6,6,6][benz], [P4,4,4,12][benz], [P4,4,4,4][benz], and 1-butyl-3-methylimidazolium hexafluorophosphate [bmim]PF_6 ionic liquids. The results are compared for IL weight fractions of 60%$_w$ and 99.5%$_w$.

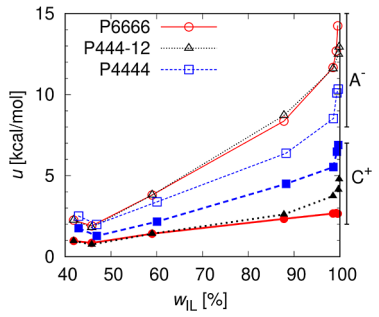

Figure 3. Comparison of the interaction energy of water with ions, $u_{H_2O-A^-}$ and $u_{H_2O-C^+}$, in three different ILs, with the ionic liquid weight fraction w_{IL} (A^- indicates anion and C^+ indicates cation). Generally, the interaction energy increases with the lower amount of absorbed water. The results are shown for the phosphonium benzoate [P6,6,6,6][benz], [P4,4,4,12][benz], and [P4,4,4,4][benz] ionic liquids.

ionic liquid. Conversely, the water and the benzoate ([benz]) anion followed an inverse trend, with their interaction energy increasing from 7 kcal/mol for [P4,4,4,4][benz] to 14 kcal/mol for [P6,6,6,6][benz], also in the 99.5%$_w$ system.

Both water−cation and water−anion interaction energy decreased in all cases with an increase of water content, e.g., a decrease in ionic liquid weight fraction w_{IL}, as shown in Figure 3. However, even at an ionic liquid weight fraction of 60%$_{w,IL}$, the interaction between water and the [P4,4,4,4] cation remained the strongest at 4.5 kcal/mol, while it was the weakest for the [P6,6,6,6] cation at 2.3 kcal/mol, cf. Figure 2. This relationship indicates that the energy of the water−cation interaction decreased with an increase in the alkyl chain length of the cation, which has been confirmed by measurements[43,44] and other modeling studies.[27] Consequently, due to the opposing trends in water interaction energies with the components of ionic liquids, all three phosphonium ionic liquids exhibited similar interaction energies with water across all investigated systems, approximately 17 kcal/mol for 99.5%$_{w,IL}$ and 11 kcal/mol for 60%$_{w,IL}$, as shown in Figure 2.

Our findings for the phosphonium ionic liquids suggest that, although the interaction energy between cations and water depends on the cation's molecular weight or molecular volume, the stronger interaction between anions and water compensates for this difference. This observation holds for a wide range of ionic liquid concentrations. The interaction energy between water and the ionic liquid is directly related (i.e., positively correlated) to ionic liquid weight fraction, decreasing to 30% of the calculated concentrated phosphonium ionic liquid values at 40%$_w$ ionic liquid content. In the case of the [bmim]PF_6 ionic liquid, the water−anion interaction energy was 10 kcal/mol, while the water−cation interaction energy was 3.5 kcal/mol for 99.5%$_{w,IL}$, making it roughly 20% weaker than the investigated phosphonium ionic liquids. This was expected since [bmim]PF_6 is immiscible with water.

A radial distribution function (RDF) analysis is conducted for phosphonium ILs using the central phosphorus (P^+) atom of the cation and the oxygen atoms of a benzoate carboxyl group and water, labeled as O^- and O_{H_2O}, respectively. This

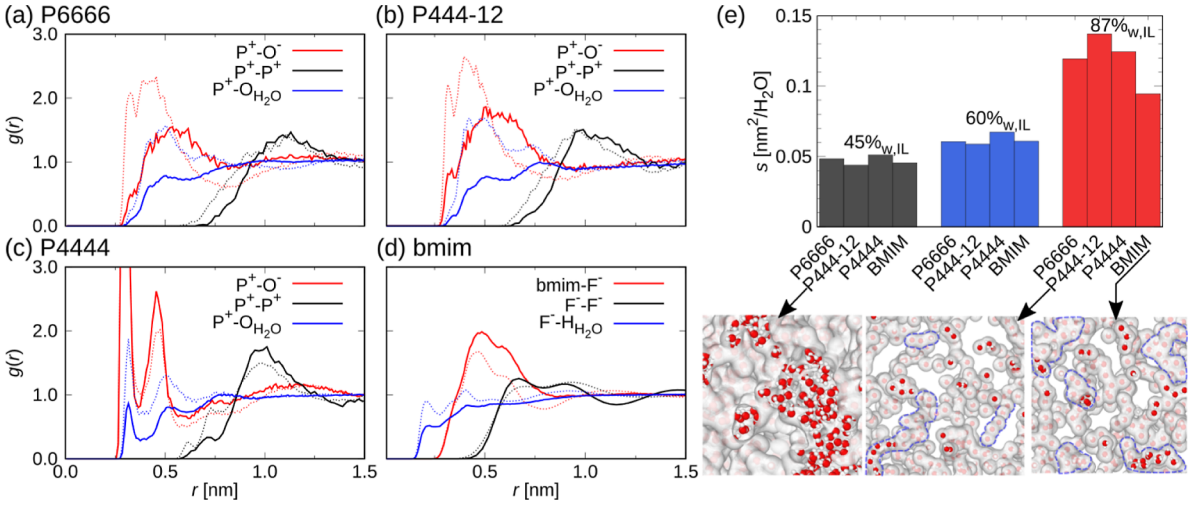

Figure 4. Radial distribution functions indicate interionic distances and ion−ion or ion−water coordination. RDFs show data for phosphonium (a) [P6,6,6,6][benz], (b) [P4,4,4,12][benz], (c) [P4,4,4,4][benz], and (d) [bmim]PF_6 ionic liquids for 87%$_{w,IL}$ and 60%$_{w,IL}$, indicated by the solid and dashed lines, respectively. (e) The specific surface of the water−ionic liquid interface is calculated as the total surface of all water pockets normalized with the number of water molecules in the system. Three lower panels show snapshots of the water clusters for [P4,4,4,12][benz] at 45%$_{w,IL}$ and 87%$_{w,IL}$ and [bmim]PF_6 at 87%$_{w,IL}$, from left to right, respectively.

https://doi.org/10.1021/acs.langmuir.4c00372
Langmuir 2024, 40, 9049−9058

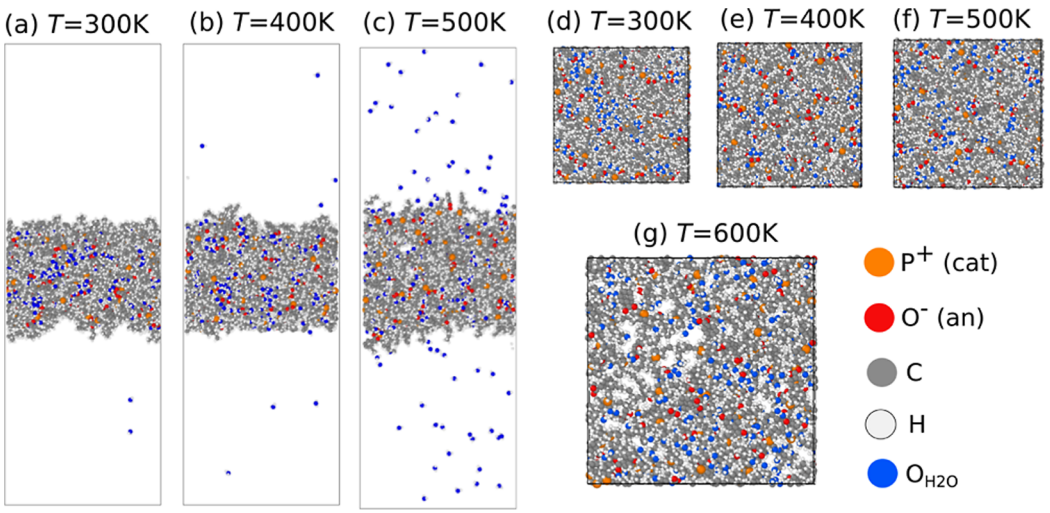

Figure 5. Snapshots of the phosphonium benzoate [P6,6,6,6][benz] 87%$_{w,IL}$ system. Evolution with the temperature of a film consisting of ionic liquid and water at the center of the simulation box, with a 5 nm vacuum added to form an interface. The snapshots of the film are shown at temperatures (a) 300, (b) 400, and (c) 500 K. The critical water behavior in bulk is shown at temperatures (d) 300, (e) 400, (f) 500, and (g) 600 K. The simulations had periodic boundary conditions in all three Cartesian coordinate directions. The temperature increased while keeping the pressure constant at 1 bar. A cation's phosphorus atom is represented as orange, an anion's oxygen is red, water's oxygen is blue, carbon atoms are gray, and hydrogens are white.

analysis provides insights into the liquid structure of ILs by examining the distribution of ions and water molecules in their environment. Figure 4a–c displays the RDFs of phosphonium cation–anion (P^+-O^-), cation–cation (P^+-P^+), and cation–water ($P^+-O_{H_2O}$) interactions for 87%$_{w,IL}$ and 60%$_{w,IL}$, indicated by the solid and dashed lines, respectively. As shown in Figure 4, a solvation shell is evident in the cation–anion interaction, with a prominent peak observed at 0.5 nm in the P^+-O^- RDF. Furthermore, it can be observed from Figure 4 that the P^+-O^- interaction is inherently stronger than the P^+-P^+ interaction. The results suggest that an increase in the water fraction leads to significant differences in the local order of anions and cations.

One notable effect of introducing more water into the system is that the peak of the P^+-O^- RDF becomes more pronounced and shifts closer to the contact distance of the van der Waals volumes, as seen in Figure 4a–c. Specifically, the pronounced peaks of the P^+-O^- RDF for [P4,4,4,4][benz] in Figure 4c originate from the oxygens of the carboxyl group (refer to Figure 1). Compared to [P6,6,6,6] molecules, the shorter chains of [P4,4,4,4] are less likely to interfere with the benzene ring to which the carboxyl group is attached in benzoate.

The radial density of water molecules near the P^+ core of the phosphonium cation increases with higher water concentration and for shorter alkyl chain lengths, cf. Figure 4a,c. This indicates that water acts as a good solvent for phosphonium alkyl chains. In this scenario, interactions between the alkyl segments and solvent molecules are energetically favorable, and additional water causes the alkyl chains to expand into a linear configuration. As the alkyl chains expand, the anions and water molecules can approach the polar core of the phosphonium cation. The RDFs of P^+-P^+ for cation–cation interactions exhibit the first peak at 1 nm, twice the length of the P^+-O^- distance. The position and height of the P^+-P^+ RDFs remain unchanged with varying amounts of water in the system, indicating that the phosphonium benzoate ionic liquid possesses a fairly stable network structure of ions spanning the system.

Figure 4d shows RDFs for [bmim]PF_6, also for two ionic liquid concentrations 87%$_{w,IL}$ and 60%$_{w,IL}$, indicated by the solid and dashed lines, respectively. The cation–anion (bmim–F^-) peak was observed at 0.48 nm, comparable to peaks in [P6,6,6,6][benz] and [P4,4,4,12][benz] ionic liquids. Interestingly, opposite to the trend observed for phosphonium, [bmim]PF_6 RDFs do not show any significant changes with water concentration in Figure 4d. The radial density at the cation–anion peak decreases only slightly with increasing water concentration. For the anion–water–water interaction, RDFs show a steady increase from 0.23 nm at 87%$_{w,IL}$, which evolves into a peak at 60%$_{w,IL}$. This peak is followed by a second water shell at 0.46 nm for 60%$_{w,IL}$ (reminiscent of [P4,4,4,4][benz] RDFs).

Analyzing the [bmim]PF_6 RDF for anion–anion (F^-F^-) interactions shows the first broadest peak at 0.53 nm, whereas the second is at 0.89 nm, approaching much closer than anions in phosphonium ionic liquids. The weak influence of water on the structure of [bmim]PF_6, visible in Figure 4d $F^-O_{H_2O}$, is expected since interaction energy between water and the [bmim]PF_6 system is weaker compared to phosphonium ionic liquids. For example, the interaction energy in the case of [bmim]PF_6 reaches 30% of the calculated phosphonium ionic liquids values at 60%$_{w,IL}$, cf. Figure 2.

In the following, we investigate the self-organization of a water–ionic liquid system at a larger scale. Already at 87%$_{w,IL}$, there are enough water molecules to create a connected network of water pockets throughout the system. This network of clusters adds a higher (microscopic) level to the water structure inside the ionic liquid. We employ the specific surface of the water–ionic liquid interface as a quantitative property of the water molecule pockets within the IL.

The specific surface is the total surface enveloping water clusters normalized by the number of water molecules in the system. To generate the surface enveloping water molecule clusters, we used a method that utilizes the superposition of 3D

https://doi.org/10.1021/acs.langmuir.4c00372
Langmuir 2024, 40, 9049–9058

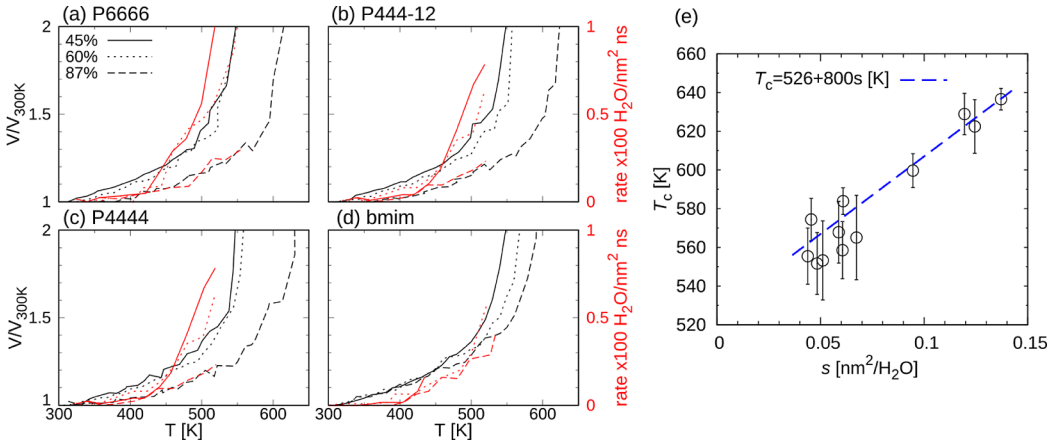

Figure 6. Evolution of volume (black) and rate of evaporation (red) with increasing temperature for ionic liquid 45%$_{w,IL}$, 60%$_{w,IL}$, and 87%$_{w,IL}$ content, indicated by the solid, dotted, and dashed lines, respectively. The panels show data for phosphonium benzoate (a) [P6,6,6,6][benz], (b) [P4,4,4,12][benz], (c) [P4,4,4,4][benz], and (d) [bmim]PF_6 ionic liquids. (e) Dependence of critical temperature T_c associated with volume expansion in panels (a–d), i.e., $V \propto e^{-T_c/T}$ on the specific surface s of the water–ionic liquid interface. The curve is obtained by a linear fit of the points.

Gaussian functions at each particle site.[45] The algorithm generates a density map by aggregating Gaussian densities on a 3D lattice within a bounding box, guaranteeing the inclusion of all particles. Two pivotal parameters shaping the isosurface morphology are the radius scaling, which adjusts the Gaussian function width based on the visible particle radius multiplied by a scaling factor (in this case, set to 1.25), and the Gaussian isosurface value, a threshold determining the distance of the contour surface from particle centers (here, set to 0.1). The chosen parameter values lead to a reduced threshold and broader particle-assigned volumes, effectively preventing the gaps within water clusters which could unphysically increase the surface.

Figure 4e shows the evolution of the normalized specific surface (s) of the water–ionic liquid interface with water concentration. The higher content of water results in a smaller contact surface to the ionic liquid, as water molecules cluster together. Conversely, the specific surface of the contact increases as the water quantity decreases.

Snapshots showing only water molecules visualize the evolution of the water network shape with ionic liquid content in Figure 4e. The increase of specific surface in case of a higher ionic liquid content is more than two times, cf. Figure 4e for 87%$_{w,IL}$. Inspection of configurations for [P4,4,4,12][benz] and [bmim]PF_6 indicates that water clusters are becoming linear, i.e., water orders into a network of elongated pockets and stays interconnected into a network. Additionally, at low water content (i.e., 87%$_{w,IL}$), there is a difference of 30% in the specific surface between phosphonium ionic liquids and the [bmim]PF_6 system. This difference can be traced to the existence of the larger water clusters in [bmim]PF_6 as opposed to phosphonium ionic liquids, denoted on snapshots in Figure 4e with dashed lines. This observation is fully in line with a weak influence of water content on the RDFs of [bmim]PF_6 and in turn its weaker interaction energy compared to the investigated phosphonium ionic liquids.

Boiling Point of Water–Ionic Liquid Systems. In this section, we examine the simulation results of water evaporation and analyze the boiling point of the water–IL system. Snapshots of the two simulation setups are shown in Figure 5.

The first set of simulations comprises a film consisting of ionic liquid and water at the center of the simulation box, with a 5 nm vacuum added to form a liquid–vapor interface. The snapshots of such an interface with [P6,6,6,6] [benz] 87%$_{w,IL}$ are shown in Figure 5a–c. MD simulations of four liquid–vapor interfaces for different ionic liquid–water solutions were carried out, and the temperature was increased in 20 K steps every 0.2 ns in the range 300–560 K. The well-defined liquid–vapor interface was observed for all ionic liquid–water systems at temperatures below 450 K. In simulations, the water molecules in the solution detached from the surface and evaporated into the vacuum, as well as, reabsorbed back into the interface, see Figure 5a–c. At 400 K, with a kinetic energy of 0.8 kcal/mol for water molecules, the surface released adsorbed water due to the molecules having sufficient kinetic energy to leave the droplet. We follow the evolution of the evaporation rate, i.e., the number of water molecules released into vacuum through the unit of surface area (28 nm^2) in a given time frame (0.2 ns).

The evaporation rate is modeled by the Arrhenius equation $k \propto e^{E_A/k_BT}$. The Arrhenius equation postulates a threshold energy governing individual collisions between molecules. These collisions result in the molecule acquiring sufficient kinetic energy to overcome adhesion to the surface and undergo evaporation. Here, based on the simulated evaporation rate, cf. Figure 6, we estimated the activation energy (E_A) for the evaporation process to be between 5 and 10 kcal/mol, which is comparable to the intermolecular binding energy. The simulated intermolecular binding energy of water and cations is approximately 2 kcal/mol, while for anions, it is around 8 kcal/mol (cf. Figure 2). Notably, the water evaporation rates increased above 400 K, ranging to quite substantial 10–50 molecules/nm^{2}ns (see Figure 6). Similar observations were made by Chaban and Prezhdo[46] for 1-butyl-3-methylimidazolium tetrafluoroborate [C_4C_1IM][BF4]-water solution, who saw a temperature increase of up to 25 K in water boiling point from vapor–liquid equilibrium. Our findings show a rapid increase in the evaporation rate at temperatures above 400 K. Furthermore, the rate of evaporation in phosphonium ionic liquids depends on the quantity of water in the system, while the film's interior

https://doi.org/10.1021/acs.langmuir.4c00372
Langmuir 2024, 40, 9049–9058

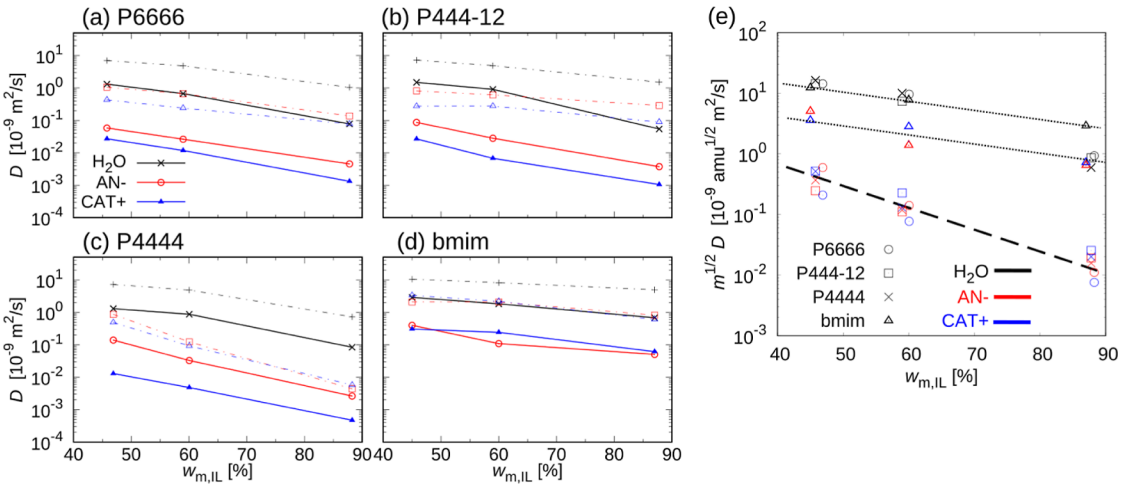

Figure 7. Dependence of the coefficient of diffusion of anions, cations, and water (H_2O) on ionic liquid content $w_{m,IL}$. The full lines are simulated at 300 K and dotted lines at 400 K. The panels show data for phosphonium (a) [P6,6,6,6], (b) [P4,4,4,12], (c) [P4,4,4,4], and (d) [bmim]PF_6 ionic liquids. (e) Evolution of the diffusion coefficient scaled with the square root of the mass of the molecule ($D \propto 1/\sqrt{m}$) for different concentrations.

remains fairly stable due to the water molecule's binding energy being 10 times higher than the kinetic energy of water molecules. One should note that Gibbs ensemble Monte Carlo simulations are necessary to fully characterize the vapor−liquid equilibria of IL−H_2O systems and mitigate the size effects.[47,48] These simulations rely on vapor−liquid phase exchange to equilibrate the chemical potential.

To investigate critical water behavior in bulk, we conduct simulations shown in the right side panels of Figure 5d−g. The simulations have periodic boundary conditions in all three Cartesian coordinate directions.

Figure 6a−d shows the evolution of the volume (V/V_{300K}) of the bulk systems with temperature. As the temperature increases in 20 K steps every 0.2 ns while keeping the pressure constant at 1 bar, the overall volume gradually expands 10−20% depending on the water/IL fraction up to temperature 500 K, keeping absorbed superheated water. The coefficient of expansion, representing the fractional change in volume per unit change in temperature, decreases from 1.4×10^{-3} K^{-1} to 0.7×10^{-3} K^{-1} for 60%$_{w,IL}$ and 87%$_{w,IL}$, respectively.

At the boiling point of the water−IL system, the liquid structure is disrupted, leading to the formation of water bubbles in the gas phase within the ionic liquid. Even in a pure water system, the surface tension of water plays a crucial role in preventing the formation and growth of bubbles until the temperature exceeds the boiling point.[49] It is therefore not surprising that the high boiling points and surface tension of ionic liquid will increase the boiling point of the mixed system compared to pure water (i.e., 273 K).

The boiling point of bulk ionic liquids is influenced by the amount of ionic liquid, which prevents rapid water expansion. Consequently, for all three phosphonium systems at low water content, i.e., 87%$_{w,IL}$, the onset of the volume expansion is delayed by about 60 K compared to the other two concentrations (45%$_{w,IL}$ and 60%$_{w,IL}$), cf. Figure 6a-c. Surprisingly, the [bmim]PF_6 system exhibits only a 20 K increase of boiling point when increasing the concentration of ionic liquid from 60%$_{w,IL}$ to 87%$_{w,IL}$, cf. Figure 6d. We observe a similar trend in water evaporation rates for [bmim]PF_6.

A possible relationship between the molecular structure of the water−ionic liquid system (analyzed in the previous section) and the critical temperature associated with an exponential volume expansion, i.e., $V \propto e^{-T_c/T}$, due to water bubble creation is outlined in Figure 6e. In particular, the specific surface of the water−ionic liquid interface could be instrumental in this, cf. Figure 4e. One can observe that a higher specific contact area of water to ionic liquid s leads to more pronounced retardation of vapor pocket formation, i.e., higher T_c. In all investigated systems, water is mixed with ionic liquid. Still, the geometry of the water pockets evolves with concentration and depends also on the molecular structure of the ionic liquid, as demonstrated in Figure 6d. To some extent, we can rely on macroscopic considerations: for the vapor pocket to expand and form a bubble, the temperature must be sufficient to generate enough vapor pressure to overcome the surface tension. This excess pressure is inversely proportional to the diameter of the bubble formed. The existence of larger water clusters, which can overcome intramolecular forces created by the strong Coulomb cohesion forces in the ionic liquid, reduces critical temperature.

One of the appealing attributes of ILs for various applications is their remarkably low volatility, e.g., high boiling point. This is important since it is sometimes erroneously claimed that ILs are nonvolatile. Rebelo et al.[50] demonstrated that ILs could undergo thermal vaporization, allowing for the estimation of boiling points and critical temperatures. Later, indirect and direct methods were employed to measure vapor pressure.[51,52] Simulations indicate that imidazolium ionic liquids have critical temperatures around 1200 K, with a decrease in critical temperature as the alkyl chain length on the cation increases, but still far above the temperatures studied here.[47,48]

In practical systems, we may encounter scenarios where water molecules are removed from the vicinity of the ionic−liquid surface. The resulting interface would experience a local rapid depletion and evaporation would be limited by the rate at which water diffuses through and between water pockets (seen in Figure 4) to the surface, an aspect we will explore in the following section.

Simulations of Diffusion in the Water−Ionic Liquid System. The diffusivity of cations, anions, and water, D_s, was investigated using the Einstein relation for molecular move-

https://doi.org/10.1021/acs.langmuir.4c00372
Langmuir 2024, 40, 9049−9058

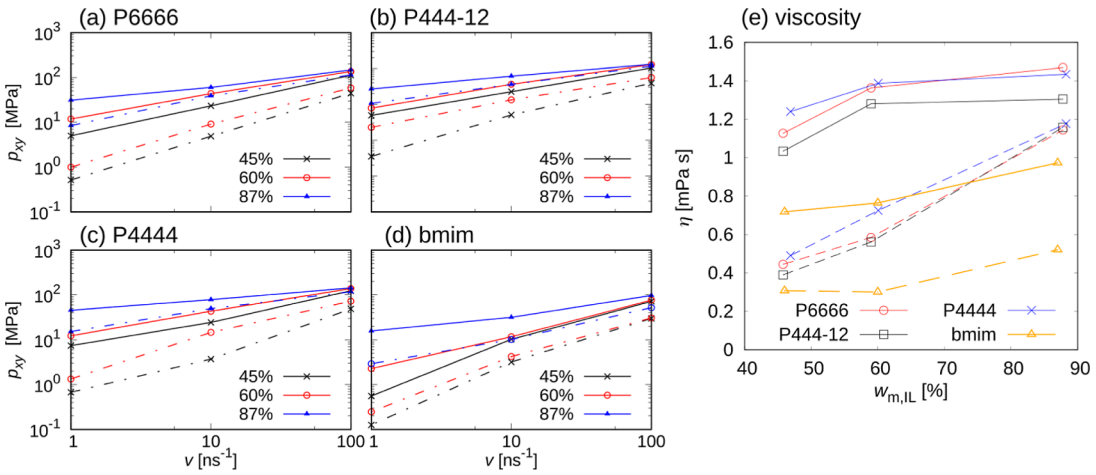

Figure 8. Dependence of shear stress p_{xy} on shear rate v for different ionic liquid contents $w_{m,IL}$. The water is denoted black, anion red, and cation blue. The panels show data for phosphonium (a) [P6,6,6,6], (b) [P4,4,4,12], (c) [P4,4,4,4], and (d) [bmim]PF_6 ionic liquids. The lines serve as a guide to the eye. (e) Dependence of viscosity $\eta = p_{xy}/v$ across all systems at v = 100 ns^{-1} on ionic liquid weight fraction $w_{m,IL}$. The solid lines in all panels are simulated at 300 K and dashed−dotted lines at 400 K.

ment in liquid, $6D_s t = \sum_{i=1}^{N} \langle (\vec{r}_i - \vec{r}_i^{\,0})^2 \rangle$, linking diffusion coefficient to the evolution with time of the mean-square of the displacement (msd) of the center of mass position $\vec{r}_i$ for each molecule (ion or water) i. The msd over time is represented by the brackets $\langle\rangle$, N denotes the number of ions, and the factor 6 accommodates the three-dimensional nature of the system. The ionic liquid simulations at 300 K are found to be mostly subdiffusive based on the observation that a linear fit to the msd as a function of time on a log−log scale has a slope <1. To compare the diffusivity of different systems, we focus on the portion of the msd curve after 1.5 ns where all systems exhibit a linear dependence of the msd on time, cf. refs 53 and 54. Using the method of least-squares on msd values, we calculate the diffusion coefficient for all systems and their different components (i.e., cations, anions, and water molecules).

From Figure 7, it can be observed that, as the mass fraction of ionic liquid increases, the diffusion coefficient D of all IL−water system components decreases. The absolute values of the ion diffusion constants, approximately 10^{-11} m^2/s, are an order of magnitude smaller than those of water at ambient temperatures and this difference increases with concentration, cf. refs 55 and 56. A most significant difference in water transport between the three phosphonium ionic liquids and [bmim]PF_6 is visible at a high ionic liquid volume fraction ($87\%_{w,IL}$). The diffusion coefficient values for water decrease by an order of magnitude with increasing concentration of phosphonium ionic liquids, from 2×10^{-8} m^2/s at a fraction of $45\%_{w,IL}$ to below 10^{-9} m^2/s at a fraction of $87\%_{w,IL}$. On the other hand, the water diffusion coefficient in [bmim]PF_6 decreases to a third of its value at $45\%_{w,IL}$, i.e., from 3×10^{-8} m^2/s to 1×10^{-8} m^2/s in the range $45\%_{w,IL}$ to $87\%_{w,IL}$, respectively. This is due to a weaker interaction energy between the ionic liquid and water, as outlined in Figure 2 and the corresponding section.

At 400 K, we observe that, for all investigated ionic liquids, the diffusion coefficient decreases with increasing ionic liquid concentration $w_{w,IL}$ to a third of its value at $45\%_{w,IL}$. The self-diffusion coefficients at 400 K are an order of magnitude higher than at 300 K. Such an increase in mobility cannot be explained solely by an increase in thermal velocity ($v_{therm} \propto \sqrt{T}$) but also indicates a change in dynamics of water association with ionic liquid and other water molecules due to temperature.

One can observe that the slope of the diffusion rate D with IL content $w_{w,IL}$ at 300 K is similar for all phosphonium anions and cations independent of their cationic alkyl chain lengths. On the other hand, cation's structure changes the evolution of diffusion rate with the concentration of ionic liquid at 400 K. The two phosphonium liquids with higher alkyl group content [P6,6,6,6] and [P4,4,4,12] exhibit higher diffusional mobility compared to [P4,4,4,4], cf. Figure 7a−c, especially at high ionic liquid concentrations. This indicates that alkyl group content is a tuning parameter for strong Coulomb interactions between the central phosphorus atom in the cation and oxygen of the anion molecule. Figure 7e shows the scaling of the diffusion coefficient with the square root of the mass of the molecule ($D \propto 1/\sqrt{m}$). The water behaves similarly in all four systems and the three phosphonium benzoate pairs also follow a similar trend. In contrast, [bmim]PF_6 is more mobile than the phosphonium ionic liquids, with the diffusion being an order of magnitude larger when corrected for its mass.

Water−IL System under Shear. We calculated the shear stress evolution with shear rate through nonequilibrium molecular dynamics simulations in a box with periodic boundary conditions. In bulk simulations, the entire simulation box undergoes shear, causing changes in its shape. The simulation box's deformation and the subtraction of a velocity bias due to deformation, i.e., the shear-induced velocity of flow, are accomplished with the SLLOD thermostat.[57,58]

The results reveal that shear stress decreases with rising temperature across all systems, as shown in Figure 8a−d. The change in shear stress with temperature is particularly pronounced in the case of the [bmim]PF_6 ionic liquid and low ionic liquid content ($45\%_{w,IL}$). Weak interaction of water with [bmim]PF_6 results in almost 50% lower shear stress than that of the phosphonium ionic liquids. Further, viscosity is lower for the asymmetric phosphonium cation molecule [P4,4,4,12] compared to the symmetric one [P6,6,6,6]. Higher symmetry facilitates close packing, promoting increased ionic interaction, compared to interactions with water, as observed in the energies in Figure 2 and contact surface in Figure 4e, cf. also ref 59.

https://doi.org/10.1021/acs.langmuir.4c00372
Langmuir 2024, 40, 9049−9058

The viscosity $\eta = p_{xy}/\nu$ is calculated across all systems at the highest shear rate $\nu = 100\ ns^{-1}$ and depicted in Figure 8e. The results demonstrate that an increase in water content leads to a decrease in viscosity across all systems. This observation suggests two considerations: first, since water is less viscous than ionic liquids, the addition of water is expected to lower the overall viscosity. Second, in alignment with the results for interaction energy, diffusion rate, and boiling point, the presence of water molecules decreases the strength of interactions between ions. These weaker interactions result in higher mobility of cations and anions and yield less viscous solutions at higher water content.

Closer inspection of Figure 8a−d indicates the presence of shear thinning in all ionic liquids at 300 K, described by a power law function with an exponent smaller than one, $p_{xy} \propto \nu^n$ and $n < 1$. For our systems, the exponent at $87\%_{w,IL}$ and 300 K is $n = 0.25$ for [P4444], $n = 0.35$ for [P444−12] and [P6666], and $n = 0.4$ for [bmim]. The addition of water reduces the effect of shear thinning, increasing the exponents. The most striking change occurs for $[bmim]PF_6$, which, according to our simulations, recovers its viscous behavior at elevated water amounts ($45\%_{w,IL}$, cf. Figure 8d). At 400 K and for ionic liquid content $w_{IL} \leq 60\%_{w,IL}$, the symmetric cation phosphonium [P4,4,4,4][benz] and [P6,6,6,6][benz] ionic liquids as well as imidazolium $[bmim]PF_6$ ionic liquid recover viscous shear stress dependence on the shear rate ($n = 1$).

When considering how water alters the lubricating properties of the ionic liquid, it is crucial to acknowledge the significant role played by the interaction of water with solid interfaces (see ref 36). In small quantities, water resists slip and increases friction; however, intriguingly, this tendency slightly reverses with higher water content.[60,61] Additionally, water can accumulate on surfaces, via diffusion as it strongly adheres to charged surfaces. We find that the diffusion rate of a specific ionic liquid is independent of its molecular structure and solely dependent on the water content. Consequently, the presence of water can pose a significant practical concern, particularly in systems where controlling the friction or electrochemical reactions is important.

CONCLUSIONS

We have investigated the behavior of phosphonium ionic liquids, trying to link their molecular structure to their thermodynamic and kinetic behavior. The distinctive structural features of phosphonium ionic liquids, particularly the cationic alkyl chain length, molecular symmetry, and the consequential tuning of Coulomb interactions, have emerged as key determinants influencing their dynamic behavior. Our findings underscore the intricate relationship between water content and the rate of evaporation in phosphonium ionic liquids. In addition to the remarkable stability of bulk ionic liquid-water solutions attributed to the substantial binding energy of water molecules to the ionic liquid and high surface tension, evaporation is affected by the amount of water within the system. The interplay between molecular interactions that suppress evaporation and retard the transition from liquid to gas is highlighted. With respect to diffusion, our investigation has delineated temperature-dependent trends in three phosphonium benzoate ionic liquids. The scaling of the diffusion coefficient with the square root of molecule mass further elucidates the influence of molecular weight on the diffusion dynamics of these systems. The comparison with a reference $[bmim]PF_6$ ionic liquid highlights the latter's exceptional mobility, surpassing phosphonium ionic liquids by an order of magnitude when corrected for mass. Concerning the connection between molecular interactions, water content, and viscosity, the increase in water content correlates consistently with a decrease in viscosity across all systems. This phenomenon underscores the significant role of water molecules in weakening interactions between ions.

This study supports the continued development of phosphonium-based room-temperature ionic liquids that are emerging as promising environmentally friendly lubricants, distinguished by their simple synthesis process. With high viscosity, high thermal stability, and low vapor pressure, ionic liquids exhibit a versatile nature that promotes them as lubricants of choice for challenging and inaccessible operational environments. The variability of their properties, influenced by factors like cation alkyl chain length and the choice of anion, introduces customization possibilities. The potential for establishing a circular economy is underscored by their biodegradability, paving the way for recovery and reusability, not only in lubrication, but also across diverse domains, spanning from battery electrolyte development to CO_2 reduction. Continuing research focused on linking their molecular, microscale, and thermodynamic properties will potentially enable tuning of properties to meet specific application requirements.

AUTHOR INFORMATION

Corresponding Author

Igor Stanković − *Scientific Computing Laboratory, Center for the Study of Complex Systems, Institute of Physics Belgrade, University of Belgrade, Belgrade 11080, Serbia;* orcid.org/0000-0001-5756-7196; Email: igor.stankovic@ipb.ac.rs

Authors

Miljan Dašić − *Scientific Computing Laboratory, Center for the Study of Complex Systems, Institute of Physics Belgrade, University of Belgrade, Belgrade 11080, Serbia;* orcid.org/0000-0002-1739-0784

Mateja Jovanović − *Scientific Computing Laboratory, Center for the Study of Complex Systems, Institute of Physics Belgrade, University of Belgrade, Belgrade 11080, Serbia*

Ashlie Martini − *Department of Mechanical Engineering, University of California, Merced, California 95343, United States;* orcid.org/0000-0003-2017-6081

Complete contact information is available at: https://pubs.acs.org/10.1021/acs.langmuir.4c00372

Notes

The authors declare no competing financial interest.

ACKNOWLEDGMENTS

I.S., M.D., and M.J. acknowledge the support of the Ministry of Science, Technological Development, and Innovation of the Republic of Serbia, through the Institute of Physics Belgrade. I.S. gratefully acknowledges financial support from the Fulbright Visiting Scholar Program for his visit to the University of California Merced. Numerical calculations were run on the PARADOX supercomputing facility at the Scientific Computing Laboratory of the Institute of Physics Belgrade. I.S. is grateful to Ting Liu for the fruitful discussions and advice.

https://doi.org/10.1021/acs.langmuir.4c00372
Langmuir 2024, 40, 9049−9058

REFERENCES

(1) Dold, C.; Amann, T.; Kailer, A. Influence of structural variations on imidazolium-based ionic liquids. *Lubric. Sci.* **2013**, *25*, 251−268.
(2) Dašić, M.; Stanković, I.; Gkagkas, K. Molecular dynamics investigation of the influence of the shape of the cation on the structure and lubrication properties of ionic liquids. *Phys. Chem. Chem. Phys.* **2019**, *21*, 4375−4386.
(3) Zhou, F.; Liang, Y.; Liu, W. Ionic liquid lubricants: designed chemistry for engineering applications. *Chem. Soc. Rev.* **2009**, *38*, 2590−2599.
(4) Hayes, R.; Warr, G. G.; Atkin, R. At the interface: solvation and designing ionic liquids. *Phys. Chem. Chem. Phys.* **2010**, *12*, 1709−1723.
(5) Gkagkas, K.; Ponnuchamy, V.; Dašić, M.; Stanković, I. Molecular dynamics investigation of a model ionic liquid lubricant for automotive applications. *Tribol. Int.* **2017**, *113*, 83−91.
(6) Liu, T.; Panwar, P.; Khajeh, A.; Rahman, M. H.; Menezes, P. L.; Martini, A. Review of Molecular Dynamics Simulations of Phosphonium Ionic Liquid Lubricants. *Tribol. Lett.* **2022**, *70*, 44.
(7) Aparicio, S.; Atilhan, M. Mixed Ionic Liquids: The Case of Pyridinium-Based Fluids. *J. Phys. Chem. B* **2012**, *116*, 2526−2537.
(8) Scarbath-Evers, L. K.; Hunt, P. A.; Kirchner, B.; MacFarlane, D. R.; Zahn, S. Molecular features contributing to the lower viscosity of phosphonium ionic liquids compared to their ammonium analogues. *Phys. Chem. Chem. Phys.* **2015**, *17*, 20205−20216.
(9) Rahman, M. H.; Khajeh, A.; Panwar, P.; Patel, M.; Martini, A.; Menezes, P. L. Recent progress on phosphonium-based room temperature ionic liquids: Synthesis, properties, tribological performances and applications. *Tribol. Int.* **2022**, *167*, 107331.
(10) Pensado, A.; Comunas, M.; Fernández, J. The pressure−viscosity coefficient of several ionic liquids. *Tribol. Lett.* **2008**, *31*, 107−118.
(11) Minami, I.; Kita, M.; Kubo, T.; Nanao, H.; Mori, S. The Tribological Properties of Ionic Liquids Composed of Trifluorotris(pentafluoroethyl) Phosphate as a Hydrophobic Anion. *Tribol. Lett.* **2008**, *30*, 215−223.
(12) Minami, I. Ionic liquids in tribology. *Molecules* **2009**, *14*, 2286−2305.
(13) Cai, M.; Yu, Q.; Liu, W.; Zhou, F. Ionic liquid lubricants: when chemistry meets tribology. *Chem. Soc. Rev.* **2020**, *49*, 7753−7818.
(14) Bou-Malham, I.; Bureau, L. Nanoconfined ionic liquids: effect of surface charges on flow and molecular layering. *Soft Matter* **2010**, *6*, 4062−4065.
(15) Beattie, D. A.; Espinosa-Marzal, R. M.; Ho, T. T.; Popescu, M. N.; Ralston, J.; Richard, C. J.; Sellapperumage, P. M.; Krasowska, M. Molecularly-thin precursor films of imidazolium-based ionic liquids on mica. *J. Phys. Chem. C* **2013**, *117*, 23676−23684.
(16) Wang, Z.; Priest, C. Impact of nanoscale surface heterogeneity on precursor film growth and macroscopic spreading of [Rmim][NTf2] ionic liquids on mica. *Langmuir* **2013**, *29*, 11344−11353.
(17) Oster, K.; Goodrich, P.; Jacquemin, J.; Hardacre, C.; Ribeiro, A.; Elsinawi, A. A new insight into pure and water-saturated quaternary phosphonium-based carboxylate ionic liquids: Density, heat capacity, ionic conductivity, thermogravimetric analysis, thermal conductivity and viscosity. *J. Chem. Thermodyn.* **2018**, *121*, 97−111.
(18) Sheridan, Q. R.; Schneider, W. F.; Maginn, E. J. Anion Dependent Dynamics and Water Solubility Explained by Hydrogen Bonding Interactions in Mixtures of Water and Aprotic Heterocyclic Anion Ionic Liquids. *J. Phys. Chem. B* **2016**, *120*, 12679−12686.
(19) Wu, H.; Maginn, E. J. Water solubility and dynamics of CO2 capture ionic liquids having aprotic heterocyclic anions. *Fluid Phase Equilib.* **2014**, *368*, 72−79.
(20) Zhao, Y.; Tian, L.; Pei, Y.; Wang, H.; Wang, J. Effect of Anionic Structure on the LCST Phase Behavior of Phosphonium Ionic Liquids in Water. *Ind. Eng. Chem. Res.* **2018**, *57*, 12935−12941.
(21) Venkatesan, S. S.; Huda, M. M.; Rai, N. Molecular insights into ionic liquid/aqueous interface of phosphonium based phase-separable ionic liquids. *AIP Adv.* **2019**, *9*, 045115.
(22) Pivnic, K.; Bresme, F.; Kornyshev, A. A.; Urbakh, M. Structural Forces in Mixtures of Ionic Liquids with Organic Solvents. *Langmuir* **2019**, *35*, 15410−15420.
(23) McDaniel, J. G.; Verma, A. On the Miscibility and Immiscibility of Ionic Liquids and Water. *J. Phys. Chem. B* **2019**, *123*, 5343−5356.
(24) Liu, W.; Zhao, T.; Zhang, Y.; Wang, H.; Yu, M. The Physical Properties of Aqueous Solutions of the Ionic Liquid [BMIM][BF4]. *J. Solution Chem.* **2006**, *35*, 1337−1346.
(25) Sturlaugson, A. L.; Fruchey, K. S.; Fayer, M. D. Orientational Dynamics of Room Temperature Ionic Liquid/Water Mixtures: Water-Induced Structure. *J. Phys. Chem. B* **2012**, *116*, 1777−1787.
(26) Feng, S.; Voth, G. A. Molecular Dynamics Simulations of Imidazolium-Based Ionic Liquid/Water Mixtures: Alkyl Side Chain Length and Anion Effects. *Fluid Phase Equilib.* **2010**, *294*, 148−156.
(27) Klähn, M.; Stüber, C.; Seduraman, A.; Wu, P. What Determines the Miscibility of Ionic Liquids with Water? Identification of the Underlying Factors to Enable a Straightforward Prediction. *J. Phys. Chem. B* **2010**, *114*, 2856−2868.
(28) Niazi, A. A.; Rabideau, B. D.; Ismail, A. E. Effects of water concentration on the structural and diffusion properties of imidazolium-based ionic liquid-water mixtures. *J. Phys. Chem. B* **2013**, *117*, 1378−1388.
(29) Blahušiak, M.; Schlosser, S. ˇ. Physical properties of phosphonium ionic liquid and its mixtures with dodecane and water. *J. Chem. Thermodyn.* **2014**, *72*, 54−64.
(30) Jorgensen, W. L.; Maxwell, D. S.; Tirado-Rives, J. Development and testing of the OPLS all-atom force field on conformational energetics and properties of organic liquids. *J. Am. Chem. Soc.* **1996**, *118*, 11225−11236.
(31) Dodda, L. S.; Cabeza de Vaca, I.; Tirado-Rives, J.; Jorgensen, W. L. LigParGen web server: an automatic OPLS-AA parameter generator for organic ligands. *Nucleic Acids Res.* **2017**, *45*, W331−W336.
(32) Vega, C.; de Miguel, E. Surface tension of the most popular models of water by using the test-area simulation method. *J. Chem. Phys.* **2007**, *126*, 154707.
(33) Chatterjee, S.; Debenedetti, P. G.; Stillinger, F. H.; Lynden-Bell, R. M. A computational investigation of thermodynamics, structure, dynamics and solvation behavior in modified water models. *J. Chem. Phys.* **2008**, *128*, 124511.
(34) Lorentz, H. A. Ueber die Anwendung des Satzes vom Virial in der kinetischen Theorie der Gase. *Ann. Phys.* **1881**, *248*, 127−136.
(35) Allen, M. P.; Tildesley, D. J. *Computer Simulation of Liquids*; Oxford University Press, 2017.
(36) Feng, G.; Jiang, X.; Qiao, R.; Kornyshev, A. A. Water in Ionic Liquids at Electrified Interfaces: The Anatomy of Electrosorption. *ACS Nano* **2014**, *8*, 11685−11694.
(37) Martins, V. L.; Nicolau, B. G.; Urahata, S. M.; Ribeiro, M. C. C.; Torresi, R. M. Influence of the Water Content on the Structure and Physicochemical Properties of an Ionic Liquid and Its Li+ Mixture. *J. Phys. Chem. B* **2013**, *117*, 8782−8792.
(38) Mao, Y.; Zhang, Y. Thermal conductivity, shear viscosity and specific heat of rigid water models. *Chem. Phys. Lett.* **2012**, *542*, 37−41.
(39) Mahoney, M. W.; Jorgensen, W. L. Diffusion constant of the TIP5P model of liquid water. *J. Chem. Phys.* **2001**, *114*, 363−366.
(40) Plimpton, S. Fast parallel algorithms for short-range molecular dynamics. *J. Comput. Phys.* **1995**, *117*, 1−19.
(41) Evans, D. J.; Holian, B. L. The Nose−Hoover thermostat. *J. Comput. Phys.* **1985**, *83*, 4069−4074.
(42) Spreiter, Q.; Walter, M. Classical molecular dynamics simulation with the Velocity Verlet algorithm at strong external magnetic fields. *J. Comput. Phys.* **1999**, *152*, 102−119.
(43) Huddleston, J. G.; Visser, A. E.; Reichert, W. M.; Willauer, H. D.; Broker, G. A.; Rogers, R. D. Characterization and comparison of hydrophilic and hydrophobic room temperature ionic liquids incorporating the imidazolium cation. *Green Chem.* **2001**, *3*, 156−164.

https://doi.org/10.1021/acs.langmuir.4c00372
Langmuir 2024, 40, 9049−9058

(44) Cammarata, L.; Kazarian, S. G.; Salter, P. A.; Welton, T. Molecular states of water in room temperature ionic liquids. *Phys. Chem. Chem. Phys.* **2001**, *3*, 5192−5200.
(45) Krone, M.; Stone, J.; Ertl, T.; Schulten, K. Fast Visualization of Gaussian Density Surfaces for Molecular Dynamics and Particle System Trajectories. *EuroVis-Short Papers*, 2012.
(46) Chaban, V. V.; Prezhdo, O. V. Water Phase Diagram Is Significantly Altered by Imidazolium Ionic Liquid. *J. Phys. Chem. Lett.* **2014**, *5*, 1623−1627.
(47) Rai, N.; Maginn, E. J. Vapor−Liquid Coexistence and Critical Behavior of Ionic Liquids via Molecular Simulations. *J. Phys. Chem. Lett.* **2011**, *2*, 1439−1443.
(48) Rai, N.; Maginn, E. J. Critical behaviour and vapour-liquid coexistence of 1-alkyl-3-methylimidazolium bis-(trifluoromethylsulfonyl)amide ionic liquids via Monte Carlo simulations. *Faraday Discuss.* **2012**, *154*, 53−69.
(49) Dergarabedian, P. The Rate of Growth of Vapor Bubbles in Superheated Water. *J. Appl. Mech.* **1953**, *20*, 537−545.
(50) Rebelo, L. P. N.; Canongia Lopes, J. N.; Esperança, J. M. S. S.; Filipe, E. On the Critical Temperature, Normal Boiling Point, and Vapor Pressure of Ionic Liquids. *J. Phys. Chem. B* **2005**, *109*, 6040−6043.
(51) Paulechka, Y.; Zaitsau, D. H.; Kabo, G.; Strechan, A. Vapor pressure and thermal stability of ionic liquid 1-butyl-3-methylimidazolium Bis(trifluoromethylsulfonyl)amide. *Thermochim. Acta* **2005**, *439*, 158−160.
(52) Earle, M. J.; Esperança, J. M.; Gilea, M. A.; Canongia Lopes, J. N.; Rebelo, L. P.; Magee, J. W.; Seddon, K. R.; Widegren, J. A. The distillation and volatility of ionic liquids. *Nature* **2006**, *439*, 831−834.
(53) Doherty, B.; Zhong, X.; Gathiaka, S.; Li, B.; Acevedo, O. Revisiting OPLS Force Field Parameters for Ionic Liquid Simulations. *J. Chem. Theory Comput.* **2017**, *13*, 6131−6145.
(54) Kowsari, M. H.; Alavi, S.; Ashrafizaadeh, M.; Najafi, B. Molecular dynamics simulation of imidazolium-based ionic liquids. I. Dynamics and diffusion coefficient. *J. Chem. Phys.* **2008**, *129*, 224508.
(55) Shaikh, A. R.; Ashraf, M.; AlMayef, T.; Chawla, M.; Poater, A.; Cavallo, L. Amino acid ionic liquids as potential candidates for CO2 capture: Combined density functional theory and molecular dynamics simulations. *Chem. Phys. Lett.* **2020**, *745*, 137239.
(56) Devanathan, R.; Venkatnathan, A.; Rousseau, R.; Dupuis, M.; Frigato, T.; Gu, W.; Helms, V. Atomistic Simulation of Water Percolation and Proton Hopping in Nafion Fuel Cell Membrane. *J. Phys. Chem. B* **2010**, *114*, 13681−13690.
(57) Evans, D. J.; Morriss, G. Nonlinear-response theory for steady planar Couette flow. *Phys. Rev. A: At., Mol., Opt. Phys.* **1984**, *30*, 1528−1530.
(58) Daivis, P. J.; Todd, B. A simple, direct derivation and proof of the validity of the SLLOD equations of motion for generalized homogeneous flows. *J. Chem. Phys.* **2006**, *124*, 194103.
(59) Barnhill, W. C.; Qu, J.; Luo, H.; Meyer, H. M. I.; Ma, C.; Chi, M.; Papke, B. L. Phosphonium-Organophosphate Ionic Liquids as Lubricant Additives: Effects of Cation Structure on Physicochemical and Tribological Characteristics. *ACS Appl. Mater. Interfaces* **2014**, *6*, 22585−22593.
(60) Fajardo, O. Y.; Bresme, F.; Kornyshev, A. A.; Urbakh, M. Water in Ionic Liquid Lubricants: Friend and Foe. *ACS Nano* **2017**, *11*, 6825−6831.
(61) Noël, O.; Mazeran, P.-E.; Stanković, I. Nature of Dynamic Friction in a Humid Hydrophobic Nanocontact. *ACS Nano* **2022**, *16*, 10768−10774.

https://doi.org/10.1021/acs.langmuir.4c00372
Langmuir 2024, 40, 9049−9058